Compatibilization and Toughening of Biodegradable Poly (Lactic Acid) / Cellulose Acetate Films by Polyamide Amine Dendrimers

Yansong Huang
Beijing Technology and Business University
Yu juan Jin (jinyujuan@th.btbu.edu.cn)
Beijing Technology and Business University https://orcid.org/0000-0001-7366-5810
Bo Wang
Beijing Technology and Business University
Huafeng Tian
Beijing Technology and Business University
Yunxuan Weng
Beijing Technology and Business University
Shuang Men
Beijing Technology and Business University

Research Article

Keywords: Polyamide-amine (PAMAM) Dendrimer, PLA, CA, Compatibility, Biodegradable

Posted Date: August 10th, 2021

DOI: https://doi.org/10.21203/rs.3.rs-755422/v1

Abstract

Due to the poor compatibility caused by the large difference in hydrophilicity and interface between polylactic acid (PLA) and cellulose acetate (CA), the blending of the two materials is difficult and the application is limited. To solve this problem, a type of polyamide amine (PAMAM) dendrimer was introduced to modify PLA / CA blends in this work. The results showed that PAMAM could improve the compatibility of PLA / CA blends, promote the distribution of CA and crystallization of PLA. At the same time, adding PAMAM could enhance the mechanical properties of the blend material, and the toughness and tear strength were increased by 551% and 141%, respectively. In addition, the incorporation of PAMAM increased hydrophobicity and oxygen permeability of PLA/ CA blends, and the oxygen permeability could be increased by up to 3 orders of magnitude. Degradation test results showed that the blend exhibited good biodegradability. The overall performance of the PLA/ CA blend film was optimal when the content of PAMAM was 3 phr. The biodegradable blend films with excellent performance provided wide application prospect in the food green packaging fields.

1 Introduction

Polylactic acid (PLA) is a type of thermoplastic aliphatic polyester, which is completely biodegradable and has good biocompatibility [1]. Polylactic acid can be obtained from biomass materials (cassava, sugar beet, sugarcane, etc.) fermented by microorganisms, and exhibit many fascinating properties, such as great mechanical properties and excellent fabricability [2]. However, due to the semi-rigid structure of PLA molecular segment, the intermolecular entanglement is limited, resulting in the low flexibility and crystallinity and obvious brittleness at room temperature, which greatly limits their application [3].

To improve the performance of PLA, strengthening and toughening are necessary. Physical blending of polylactic acid with other materials is the most convenient and effective method, while blending with bio-based materials can produce environmentally friendly materials with low impact on the environment. Natural cellulose is the most abundant bio-based material in the world. It is rich in source, low in price, wide in distribution and biodegradable in natural environment. Blending cellulose or cellulose derivative with PLA can improve the mechanical properties [4], thermal properties [5], hydrophilicity and crystallization ability [6]. Cellulose acetate (CA) is one of the most commercially available cellulose derivatives and has been widely used in thermoplastic composites, especially in improving thermal and mechanical properties of PLA and reducing costs [7]. The blend possesses wide applications in medical supplies and food packaging, such as antibacterial 3D printed scaffolds [8], wound dressings [9] and food cling films [10].

Although many hydroxyl groups on cellulose have been esterified by acetic acid to improve its compatibility with PLA, the remaining hydroxyl groups cause the CA to agglomerate easily and prevent the uniform dispersion of CA in PLA. At present, the compatibilization modification of PLA / CA blends includes grafting maleic anhydride on PLA[11], grafting long aliphatic chain on cellulose acetate [12], introducing the third component poly(hydroxyalkanoate) [13], PLA-g-CA graft copolymer [14], comb

copolymer [15], transesterification agent to form PLA-co-CA copolymer [16], organic clay [17], etc. However, these modification methods still have some problems, such as complicated process, difficult control, limited effect and large dosage, etc.

Polyamide amine (PAMAM) dendrimer exhibits spherical structure, contains many active surface functional groups and cavities, and its size, shape, molecular weight and number of functional groups can be precisely controlled [18]. PAMAM has biocompatibility and biodegradability [19], and can be used in biomedical, sensing, water treatment and other fields, such as anti-tumor targeted drug and gene carriers [20], bio-adhesives [21], water purification material [22] and water/oil separation membranes [23]. Due to its high activity surface functional groups, internal cavity, and low viscosity, it can be combined with a variety of molecules to produce strong chemical bonds and hydrogen bonds, which can strengthen the matrix and improve the interfacial compatibility between various substances and matrix [24, 25]. PAMAM has the characteristics of low dosage and easy process control as a compatibilizer. Different compatibilizers can be obtained by adjusting branch degree and terminal groups. In addition, PAMAM can improve the toughness and crystallinity of the matrix by physical effect rather than chemical structure change. For example, the toughness of PBAT was improved by hydrogen bonding, energy absorption in the cavity and spherical structure of PAMAM [26]. PAMAM could be used as a nucleating agent to improve the nucleation density and crystallization rate of PLA [27].

In this study, the 5.5th generation PAMAM dendrimer (PAMAM-G5.5) containing ester ends was used to improve the compatibility and physical properties of PLA / CA blend films. The amino group on PAMAM formed strong hydrogen bond with ester group and hydroxyl group on PLA and cellulose acetate, which improved the interfacial compatibility and increased the distribution of CA, resulting in the improved mechanical properties and gas barrier capability, accelerated the degradation rate. The PLA / CA blend films with a small amount of PAMAM exhibited high performance and degradability, and possess wide application as gas barrier material in food packaging areas.

2. Experimental Methods

2.1 Materials

PLA (REVODE110, $\overline{M}_w$ = 3.5 × 10^5 g · mol^{-1}, DI = 2.5) was purchased from Zhejiang Haizheng Co., Ltd. Cellulose diacetate (acetyl group of 40%) was purchased from Shanghai Yuanye Bio-Technology Co., Ltd. Dichloromethane and acetone were obtained from Maclean biochemical Technology Co. Ltd. PAMAM-G5.5 was prepared in our group according to the published method [24]. The structure of PAMAM dendrimer is shown in **Fig. 1**a- **1**b.

2.2 Preparation of PLA / CA blend films

PLA and CA (70:30, weight ratio) were dissolved in a solvent mixture of dichloromethane and acetone (8:2, v:v) under vigorous stirring for 3 hours at 30 ℃ with a magnetic stirrer. After dissolved completely, different content of PAMAM was added into the solvent and stirred vigorously using a magnetic stirrer for

5 hours. Then the mixed solution was cast into a glass mold with a size of 15 mm × 15 mm × 5 mm and drained using a glass rod to restrain the generation of air bubbles in the solution, which could ensure the intact shape of the blend films. After drying at room temperature for 24 h, the PLA / CA blend films were obtained and then further dried at 30 °C under vacuum condition to remove residual solvents.

2.3 Characterization

The structure of PLA / CA blends was tested by FT-IR Spectrometer (Model 205 Nicolet, Thermo Fisher Scientific, USA) with a wavelength between 500 and 4000 cm^{-1} and a resolution of 4 cm^{-1} with 16 scans through the KBr tableting method.

The fracture surface morphology of the blends was observed under Scanning electron microscopy (QUATA 250, FEI, USA). Before observation, the film was coated by gold through vacuum coater under a working voltage of 15 kV. SEM images were obtained with acceleration voltage of 10 kV.

The crystallization process of the PLA /CA blends was observed under polarized light microscope (CBX51, Olympus). A small amount of sample was placed between the two cover glasses on a hot stage. It was firstly heated to 200 °C for 1 min at a heating rate of 30 °C min^{-1} to form a film and then cooled to 120 °C for 30 min at a cooling rate of 20 °C min^{-1} to observe the crystallization process.

The thermal properties of the samples were determined by differential scanning calorimetry (DSC, Q20, TA, USA). The sample was rapidly heated from room temperature to 200 °C and maintained for 3 min, followed by cooling down to 25 °C at a rate of 10 °C min^{-1} and kept at that temperature for 3 min, and finally heated to 200 °C at a heating rate of 10 °C min^{-1} for second heating scan.

The thermal stability was investigated by thermogravimetric analyzer (TA-Q50, Instrument Company, USA) under a nitrogen atmosphere, and the testing temperature ranged from room temperature to 600 °C at a heating rate of 20 °C min^{-1}.

Mechanical properties were tested by a computer-controlled electronic universal testing machine (CMT6104, MTS Industry System Co., Ltd., Shenzhen, Guangdong Province, PR China) in accordance with ISO 527-3:2018 with the crosshead speed of 10 mm min^{-1}. The spline was dumbbell shaped, with the size of 75 mm in length, 6 mm in thickness.

Tear strength of the blends was tested by a computer-controlled electronic universal testing machine (CMT6104, MTS Industry System Co., Ltd., Shenzhen, Guangdong Province, P. R. China) according to JIS K7128-3-1998. The crosshead rate was chosen as 200 mm min^{1}, and the shape and dimensions of the spline were determined according to the standard. The maximum load during the tearing is taken as the right-angle tear load, and the right-angle tear strength is calculated according to Equation 1.

$$\sigma_{tr}=\frac{P}{d} \qquad (1)$$

Where is the right-angle tear strength, kN m^{-1}; **P** is the tear load, N; **d** is the thickness of the sample, mm. Five samples were analyzed for each component in the test and the average value was reported.

The hydrophilicity was characterized by measuring the contact angle of the liquid absorbent (water) using a contact angle goniometer (OCA35, Data Physics, Germany). All tests were performed on each sample for four times at different random locations. The average value was reported.

Oxygen permeability measurements were performed by a gas permeability tester (Model: VAC-V2, Jinan Labthink Mechanical and Electrical Technology Co., Ltd., Shandong Province, P. R. China) according to ISO 2556:1974. The PLA / CA blends were cut into a round film of 10 cm in diameter by a tablet machine. The oxygen transmission rate was measured over 24 hours until it reached a steady state. For each sample, the test was performed three times under the same condition.

The elemental analysis test was performed on an elemental analyzer (Vario El Cube, Elementar Company, Germany) to measure the content of C, H, N, S elements in the sample after heating at the set temperature for 90s. Samples were taken 2-3 mg each time, and the temperature of the oxidation tube and reduction tube were set at 1150 °C and 850 °C, respectively.

2.4 Biodegradability

The prepared PLA / CA blend films were cut into 10 cm diameter discs by a cutting machine, and five specimens were prepared for each sample. Samples were placed one by one in the degradation tank with 10 cm compost material at the bottom at a distance of not less than 5 cm. Then the sample was covered with at least 10 cm compost material, sprayed with a certain amount of water, and spread with dried leaves on the top of the degradation pool to prevent water evaporation. During composting test, a certain amount of water was sprayed every 5 days and samples was took every 10 days. DSC, TGA SEM and elemental analysis were used to study the effect of PAMAM on the degradation of PLA / CA blends.

3 Results And Discussion

3.1 Interactions of PLA / CA blends

Fig. 1c- **1**d shows the FT-IR spectra of PLA / CA blends with different content of PAMAM and the wavenumbers of the characteristic peaks are listed in **Tab. S1**. It can be observed that PLA exhibited typical vibration absorption of -CH_2- at 2947 cm^{-1}, the stretching vibration absorption peak of ester carbonyl C=O at 1747 cm^{-1} and the stretching vibration absorption peak of C-O-C at 1180 cm^{-1}, 1128 cm^{-1},1078 cm^{-1} and 1041cm^{-1}, respectively. When CA was added to PLA (**Fig. 1**d), the vibration absorption peak of -CH_2- decreased from 2944 cm^{-1} to 2918 cm^{-1}, while other peaks remained almost unchanged, indicating that there might be hydrogen bond between -OH of CA and -C=O of PLA[28].

When PAMAM was added (see **Fig. 1**d), the vibration absorption peaks of -CH_2- group, C=O group and C-O-C were blue shifted, indicating the hydrogen bond interaction in the blends. At the same time, compared

with the spectra of PAMAM in **Fig. 1**c, there was no obvious N-H peak of amide bond in PLA / CA blends with PAMAM, which proved that the amino group of PAMAM formed hydrogen bond with PLA and CA. The schematic diagram of hydrogen bonding between PAMAM and PLA / CA blends and intermolecular interaction between PLA and CA were shown in **Fig. 1**e. PAMAM could form hydrogen bonds with both PAMAM and PLA, leading to the improved compatibility between the two moieties.

3.2 Morphology characterization

Fig. 2 shows the SEM images of the fracture surface of the PLA / CA blends with different PAMAM contents. As shown in **Fig. 2**a, CA exhibited a spherical shape in the PLA matrix, showing an obvious sea-island structure. The smooth surface, clear phase interface and ununiform distribution of CA spherical particles indicated limited compatibility between the two moieties. [29]. Upon addition of PAMAM (**Fig.2**(b)-(d)), it was obvious that the dispersion of CA in the PLA matrix became more uniform, the particle size decreased and the distribution became narrower (Supplementary Material **Fig. S1**). In addition, the increase of surface roughness CA indicated the improved compatibility. The blend exhibited obvious ductile fracture characteristics, which indicated that PAMAM could improve the toughness of PLA / CA blends. The addition of PAMAM destroyed the original hydrogen bond between the two phases, and produced new hydrogen bond, which improved the compatibility of CA in PLA. By reducing the diameter of dispersed particles, the interfacial adhesion was improved [30].

As shown in **Fig. 2**e- **2**f, when the content of PAMAM was greater than 3 phr, the particle size of CA particles increased and the particle size distribution was wider (**Fig. S1**), indicating the decreased dispersion effect of CA in PLA matrix. The surface roughness and voids number of PLA matrix decreased, while that of CA increased. Due to the strong intermolecular hydrogen bond between PAMAM and PLA / CA blends, the high content of PAMAM was tended to accumulate on the surface of CA, which aggravated the agglomeration of CA and increased the particle size. At the same time, the interaction between PAMAM and PLA was weakened, but the interaction with CA was enhanced, resulting in the descending compatibilization effect of PAMAM on PLA / CA blends.

3.3 Crystalline Properties

Fig. 3 shows the POM images of PLA / CA blends isothermal crystallized at 120 °C for 30 minutes. In PLA / CA blends, CA could promote the crystallization rate of PLA as a nucleating agent, but the agglomeration phenomenon inhibited the nucleation effect of CA [31]. From **Fig. 3**a, the crystal of PLA was spherulite, with a large number of nuclei generated, but the crystal size was small and most of the crystals were imperfect due to the poor crystallinity of PLA and the imperfect crystal growth. When PAMAM was added, as shown in **Fig. 3**(b) - (d), the spherulite size tended to increase, and the dispersion state was more uniform than that without PAMAM. With 5 phr PAMAM, the number of nuclei of PLA decreased greatly and the grain size became larger. As can be seen from **Fig. S2**, the average spherulite size of PLA was 147.66 μm in PLA / CA blends. With the addition of PAMAM, the spherulite size of PLA increased gradually, the average spherulite size of PLA with 5 phr PAMAM was 553.04 μm. With the addition of PAMAM, the number of nuclei in PLA spherulites decreased and the crystal size gradually

increased, indicating that the addition of PAMAM molecules inhibited the formation of PLA crystal nuclei, but promoted the growth of PLA crystals.

Because PLA / CA system was a nucleation control system, on the one hand, the addition of PAMAM dendrimer improved the dispersion of CA in PLA, which was conducive to nucleation. PAMAM with three-dimensional spherical structure can promote the movement of PLA molecular segment, reduce the free energy barrier of crystallization, promote the contact between PLA segment and crystal nucleus [32]. On the other hand, due to the high content of PAMAM dendrimer, the intermolecular force was too strong, which increased the size of CA particles and inhibited the formation of crystal nuclei, resulting in the decrease of the difficulty of nucleation and decrease of crystallinity of PLA.

3.4 Thermal Properties

Fig. 4a- **4**b shows the first cooling and second heating scan curves of the PLA / CA blends with different content of PAMAM. The obtained parameters of thermal behavior such as glass transition temperature (T_g), cold crystallization temperature (T_{cc}), melting point (T_m), crystallization enthalpy (ΔH_c) and melting enthalpy(ΔH_m) of the PLA / CA blends with different content of PAMAM were summarized in **Tab. 1**.

Fig. 4a shows that there was no crystallization peak during the cooling process because CA limited the chain movement of PLA. It can be seen from **Fig. 4**b that with the increase of PAMAM content, T_g and T_m gradually decreased to 52.83 °C and155.82 °C, respectively, T_{cc} decreased first and then increased, reaching the minimum value of 100.35 °C when the content was 3phr. It suggested that the addition of PAMAM could play a plasticizing role in accelerating the movement ability of molecular segments, reduce the hydrogen bond of CA, improve the molecular chain movement and crystallization capacity [33]. The crystallization enthalpy increased with the addition of PAMAM, while the melting enthalpy increased first and then decreased, reaching the maximum at 3 phr. This indicated that with the increase of PAMAM, the crystallinity was improved and the crystal was more stable and the optimum value was reached at 3 phr, and then the defects in the crystal began to increase and the instability increased.

Fig. 4c- **4**d shows the thermogravimetric curves and the weight loss rate of the blends with different PAMAM content. **Tab. 1** included thermal decomposition parameters such as the temperature with 5% weight loss ($T_{d5\%}$), the temperature at the maximum weight loss rate (T_{dmax}) and the residue (R_d). The weight loss of PLA / CA blends mainly occurred in the temperature range of 250 °C to 450 °C, excepted for the weight loss caused by the volatilization of moisture and residual solvents at lower temperature. In the range of 250 °C to 340°C, the curve became steep from horizontal, indicating that the PLA / CA blend began to thermal degradation. Because of the low thermal degradation temperature of PAMAM, the thermal degradation of PLA / CA blend was advanced by the addition of PAMAM. The weight loss rate of the blend film was the highest in the range of 350 °C- 380 °C. When the temperature reached 400 °C, the mass loss gradually decreased and the weight tended to be stable, indicating that the thermal decomposition of the blend was basically completed. When the temperature exceeded 450 °C, the weight of the blend had no obvious change, and the residue could be regarded as the ash content of the blend.

Compared with pure PLA / CA blend, T_{dmax} decreased first and then increased, $T_{d5\%}$ and R_d increased first and then decreased with the PAMAM addition. When PAMAM was less than 3 phr, the decrease of $T_{d5\%}$ and T_{dmax} with the addition of PAMAM indicated that the thermal stability of PAMAM was reduced due to the low decomposition temperature of PAMAM, and the increase of residue indicated that the interaction between PAMAM and PLA / CA blends was enhanced and the undecomposed component was increased. When PAMAM was 3 phr, $T_{d5\%}$ was 285.02 °C, T_{dmax} was the lowest at 354.31 °C and R_d was the highest at 8.69%, which exhibited the best thermal stability. Then with the increase of PAMAM content, $T_{d5\%}$ and T_{dmax} increased slightly and the residual decreased, indicating that the interaction between PAMAM and PLA / CA blends was strong and the decomposition was more serious.

Tab. 1 Thermal performance and thermal stability parameters of the PLA/CA blends with different content of PAMAM.

Content	T_g	T_{cc}	T_m	ΔH_c	ΔH_m	$T_{d(5\%)}$	$T_{d\ tmax}$	R_d
phr	°C	°C	°C	kJ mol^{-1}	kJ mol^{-1}	°C	°C	%
0	58.25	108. 78	159.58	20.04	20.52	336.31	378.75	7.07
1	56. 66	105.53	159.09	20.61	21.99	324.75	381.59	7.08
2	55. 09	102.63	158.05	21.30	23.96	297.51	374.42	8.68
3	54.01	100.35	157.53	21.39	24.85	285.02	354.31	8.69
4	54.60	102.16	157.23	21.85	22.57	275.42	362.78	8.25
5	52.83	101.66	155.82	22.02	22.27	279.20	361.78	6.44

3.5 Mechanical properties

Fig. 5 shows the tensile and tearing properties of PLA/ CA blends with different PAMAM contents. It can be seen that with the increase of PAMAM, the tensile strength, elongation at break, fracture energy and tearing strength all increased first and then decreased. When the content of PAMAM was 3 phr, the mechanical properties of PLA / CA blends reached the maximum, the tensile strength, elongation at break, fracture energy and tearing strength were 22.56 MPa, 14.95 %, 279.232 MJ•m^{-2} and 49.94 kN•m^{-1}, respectively, which were increased by 120 %, 183 %, 551 % and 141 % compared with PLA / CA blends. With the increase of PAMAM content, the Young's modulus of the blends decreased, indicating that the main deformation of the blends was plastic deformation, and the part with elastic deformation decreased.

PAMAM enhanced the interface compatibility between PLA and CA, reduced stress concentration, and transferred the stress to CA uniformly, thereby increasing the tensile strength. PAMAM was combined with active groups in PLA and CA to form hydrogen bond physical crosslinking, which improved the toughness and tear resistance of the blends. At the same time, PAMAM promoted the slip of the interface between

PLA and CA by increasing the molecular chain motion, and the crack propagation caused by CA stress concentration also played a toughening effect. In addition, PAMAM contained a large number of cavities, which could absorb energy during tearing and stretching, playing a role of strengthening and toughening [34]. However, when the content of PAMAM exceeded 3 phr, the overall mechanical properties of PLA / CA decreased. The strong hydrogen bond of high content of PAMAM promoted the aggregation of CA, which increased the particle size, reduced dispersion degree, restricted the movement of molecular chain, and improved the stress concentration.. As a result, both the strength and toughness of the blends were reduced.

3.6 Hydrophilicity

Fig. 6a shows the contact angle image of PLA/CA blend films. Polylactic acid is a hydrophobic material, while cellulose acetate with a certain number of hydroxyl groups is hydrophilic. The contact angle of neat PLA/CA blends was 66.3°. With the addition of PAMAM, the contact angle increases first and then decreased. When 3 phr PAMAM was added, the maximum contact angle of the blend film was 79.9 °. This was mainly due to the large number of ester end groups in the dendrimer, which improved the hydrophobicity of the blend. In addition, the wettability of the material surface is not only related to the hydrophilicity of the material, but also related to the interinterface compatibility of PLA and CA. When the amount of PAMAM was less than 3phr, the compatibility between PLA and CA was improved, and the dispersion of CA in PLA matrix was promoted, thus the contact angle and hydrophobicity of PLA / CA blends was increased. When the content of PAMAM was greater than 3 phr, the interaction between PAMAM and CA was enhanced, and the increase of CA particle size resulted the decrease of compatibility, the decrease of contact angle and the increase of hydrophilicity. The hydrophilic and hydrophobic properties of PLA / CA blend films can be adjusted by changing the addition amount of PAMAM.

3.7 Gas permeability.

Fig. 6b shows the oxygen penetration of PLA / CA blends with different PAMAM contents. With the addition of PAMAM, the oxygen permeability was firstly increased and then decreased. When 4 phr PAMAM were added, the oxygen permeability of the film reached 2.025×10^{-10} $m^3 \bullet m^{-2} \cdot (1d \cdot atm)^{-1}$, which was 3 orders of magnitude higher than that of PLA / CA blend films with 0phr PAMAM, indicating that the addition of dendritic macromolecule greatly increased the oxygen permeability of the blends.

The addition of PAMAM promoted the movement of PLA molecular chain segments, caused the change of crystallinity, leading to the change of oxygen permeability of blend film. Meanwhile, the oxygen permeability of PLA / CA blend films is related to the void of the blend. PAMAM has a spherical dendritic structure with many voids between the branched chains that facilitate the passage of oxygen. The greater the number and size of voids, the faster the oxygen permeates. When the content of PAMAM was low, the number of voids in the film increased with the increase of the content of PAMAM, and the oxygen permeability of the film increased. However, when the content of PAMAM was 5 phr, CA was

agglomerated due to the over-strong hydrogen bond of PAMAM, which resulting in the decrease of oxygen permeability.

3.8 Biodegradation Behavior

The composting experiment was carried out on PLA / CA blends, and the influence of PAMAM content on the degradation performance of the blend film was explored through morphology, thermal properties and thermal stability.

Fig. 7 shows the appearance and micromorphology of PLA / CA blend films surface during composting degradation. When the time was 10 d, the surface of PLA / CA blend films containing 1 phr and 3 phr PAMAM appeared many holes and became rough, while the surface of neat PLA / CA films had no obvious change. When the degradation time was 20 days, the blend containing 3 phr PAMAM began to disintegrate and appeared large cracks. The disintegration of the blend containing 3 phr PAMAM was more obvious at 30 days, but only a small amount of the blends with 1 phr PAMAM disintegrated and appeared cracked at that time. When the degradation time was 40 days, both the PLA / CA blends containing 1phr and 3phr PAMAM showed significantly disintegration and formed many fragments, while the blank films just started to disintegrate. It indicated that the degradation time of the blends was earlier with the increase of PAMAM.

Fig. 8 shows the micro-morphology of PLA / CA blend films surface during composting degradation. It can be clearly observed that when the degradation time was 10 days, a large crack appeared on the PLA / CA blend film containing 3 phr PAMAM, only tiny cracks appeared on the film containing 1 phr PAMAM, and no obvious change was found on the film with 0phr PAMAM. After 20d, many spherical particles appeared on the surface of all the films, the number and range of cracks on the film with 1 phr PAMAM increased, and the crack on the film with 3 phr PAMAM became deeper. On the 30th day, deep cracks appeared in the film with 1 phr and 3 phr PAMAM, while only a lot of small cracks appeared in film contained 0 phr PAMAM indicated the beginning of degradation at that time. When the degradation time was 40 days, cracks and concave-convex morphology appeared on the surface of all PLA / CA blend films and degradation occurred in all of them. It could be concluded that with the increase of PAMAM content, the degradation of PLA / CA blend film was gradually accelerated, from surface erosion to internal erosion.

As shown in **Fig. 9**a**- 9**c and **Fig. S3**, T_g, T_{cc} and T_m of the blends decreased with the increase of composting degradation time. With the increase of degradation time, the thermal parameters of PLA / CA blends containing 0 phr PAMAM decreased a little, while the T_g, T_{cc} and T_m of the blend with 1 phr PAMAM increased, and the variation range was less than that of blend with 0phr PAMAM. When the content of PAMAM was 3 phr, the decrease of thermal parameters was the most obvious, indicating that these parameters decreased with the increase of PAMAM.

The thermogravimetric curves and initial decomposition temperature (T_d) of PLA / CA blends during degradation were shown in **Fig. 9**d and **Fig. S4**. It was obvious that the T_d of PLA / CA blends decreased

with the increase of PAMAM content and degradation time, and the decrease of T_d was the most significant when the PAMAM content was 3phr.

The degradation of PLA / CA blends promoted by PAMAM had been described qualitatively. In order to quantitatively study the effect of PAMAM on the biodegradation of PLA / CA blends, the changes of carbon, hydrogen and nitrogen during the degradation were studied by using the method of element analysis. **Fig. 10** shows the change of PLA / CA with different content of PAMAM during degradation, and the ratio of carbon to hydrogen and carbon to nitrogen were listed in **Tab. 2**. It can be seen from **Fig. 10** that with the increase of degradation time, the carbon content and hydrogen content of all PLA / CA blends decreased, while the nitrogen content increased, indicating that PLA / CA blends were biodegradable. As shown in **Fig. 10**a, when the degradation time was 10 days, the C content increased with the increase of PAMAM content, which was due to the introduction of PAMAM. At the same time, the C content of PLA / CA blend with 3 phr PAMAM decreased most at 40 days, from 45.1 % to 43.7 % (decreased by 1.4 %), while that of PLA / CA blend without PAMAM (0 phr) decreased only by 0.5 %, indicating that with the increase of PAMAM content, the content of C decreased more and PLA / CA degraded faster. **Fig. 10**b showed that the addition of PAMAM reduced the reduction of H content and delayed the reduction of H, indicating that more C was consumed during the degradation process. It can be seen from **Fig. 10**c that with the increase of PAMAM content, N content increased, indicating that PAMAM was one of nitrogen source. However, the N content of PLA / CA blends containing 0 phr PAMAM is not zero, which indicated that the N element was produced by microbial decomposition of PLA / CA. At the same time, the addition of PAMAM increased the N content more, indicating that PAMAM could promote the microbial decomposition of PLA / CA and improve the degradation degree. **Tab. 2** showed that with the increase of degradation time, the C / H ratio only increased slightly, indicated that the decomposition rates of C and H were basically the same during the degradation process. The C / N ratio decreased with the extension of degradation time and the increase of PAMAM content, indicating that the degradation degree of PLA / CA increased with the increase of degradation time and PAMAM content, which confirmed that PAMAM promoted the degradation of PLA / CA.

In addition, it can be seen from **Fig. 10** and **Tab. 2** that the nitrogen content of PLA / CA blends containing 3 phr PAMAM is not more than 0.9 % during the degradation process, and its ratio to carbon content is less than 2 %, while the nitrogen content introduced by PAMAM is only 0.2 % at most.

Tab. 2 Element ratio of PLA / CA blends during degradation.

	C/H			C/N		
	0 phr	1 phr	3 phr	0 phr	1 phr	3 phr
10day	11.2	12.1	11.3	97.6	81.6	69.3
20days	11.3	12.1	11.7	89.4	74.6	61.2
30days	12.4	12.6	11.7	85.5	63.6	55.5
40days	12.7	12.7	11.8	74.0	55.4	50.6

In the process of composting, polyester degradation mainly consists of two stages: the first stage is the breakdown of ester bonds to form oligomers, and the second stage is the absorption of oligomers by microorganisms [35]. At the initial stage of degradation, due to the invasion of water, the molecular chains of polylactic acid and CA were randomly broken. PLA / CA blend films with more cracks and voids were more susceptible to water erosion and hydrolyze, resulting in lower molecular weight and enhanced mobility of molecular chains. Therefore the thermal parameter of PLA / CA blends decreased [36]. As time went on, the molecular weight of the blend film further decreased, microorganisms began to erode the film to produce CO_2 and H_2O, and gradually spread from the surface to the interior of the material, and the blend film disintegrated into small pieces. Lactic acid disappeared in the process of microbial assimilation[37].

PAMAM enhanced water erosion by increasing voids number and increasing the movement of molecular chains for decomposition and microbial erosion. In addition, because the peptide bond structure of PAMAM can be hydrolyzed and aminated, PAMAM has good biodegradability and can promote the decomposition of PLA / CA [38, 39]. When the content of PAMAM was 3 phr, the degradation effect was significant and the degradation time was shortened, indicating that the biodegradability of PLA / CA blends could be improved by using a smaller amount of PAMAM.

4 Conclusions

In this work, PLA / CA was modified with PAMAM dendrimer to increase compatibility and toughness. FT-IR showed that there was hydrogen bonding between PAMAM and PLA / CA. The addition of PAMAM could reduce the particle size of CA, improve the distribution uniformity, and strengthen the interface compatibility between CA and PLA. PAMAM could promote the growth of PLA crystal and improve the crystallinity. By adding PAMAM, the mechanical performance of PLA / CA blends was improved. The hydrophilicity and gas permeability of the blend could be adjusted by changing the amount of PAMAM. Adding a small amount of PAMAM could significantly enhance the degradation effect of PLA / CA blends and shorten the degradation time. This study is expected to provide an idea for the preparation of high performance and biodegradable food packaging materials based on cellulose derivatives and polylactic acid.

Declarations

Acknowledgements

The authors are grateful to the financial support of Beijing Young Top-notch Personnel Foundation (CIT&TCD201804030) and Beijing Key Project of Natural Science (KZ201810011017). SM acknowledges Beijing Key Laboratory of Quality Evaluation Technology for Hygiene and Safety of Plastics (Beijing Technology and Business University, Beijing 100048, China) for the award of an Open Fund (QETHSP2019004).

Declaration of interests

The authors declare that they have no known competing financial interests or personal relationships that could have appeared to influence the work reported in this paper.

References

1. P. Heidarian, T. Behzad, K. Karimi, M. Sain (2018) Properties investigation of recycled polylactic acid reinforced by cellulose nanofibrils isolated from bagasse. Polym Compos 39:3740-3749. https://doi.org/10.1002/pc.24404
2. T. Zhang, W. Han, C. Zhang, Y. Weng (2021) Effect of chain extender and light stabilizer on the weathering resistance of PBAT/PLA blend films prepared by extrusion blowing. Polym Degrad Stab 183:109455. https://doi.org/10.1016/j.polymdegradstab.2020.109455
3. V. Nagarajan, A.K. Mohanty, M. Misra (2016) Perspective on Polylactic Acid (PLA) based Sustainable Materials for Durable Applications: Focus on Toughness and Heat Resistance. ACS Sustain Chem Eng 4:2899-2916. https://doi.org/10.1021/acssuschemeng.6b00321.
4. A.A. Pérez-Fonseca, J.R. Robledo-Ortíz, R. González-Núñez, D. Rodrigue (2016) Effect of thermal annealing on the mechanical and thermal properties of polylactic acid–cellulosic fiber biocomposites. J Appl Polym Sci 133. https://doi.org/10.1002/app.43750
5. C.A. Murphy, M.N. Collins (2018) Microcrystalline cellulose reinforced polylactic acid biocomposite filaments for 3D printing. Polym Compos 39:1311-1320. https://doi.org/10.1002/pc.24069
6. K. Sheng, S. Zhang, S. Qian, C.A. Fontanillo Lopez (2019) High-toughness PLA/Bamboo cellulose nanowhiskers bionanocomposite strengthened with silylated ultrafine bamboo-char. Compos B Eng 165:174-182. https://doi.org/10.1016/j.compositesb.2018.11.139
7. P. Willberg-Keyrilainen, H. Orelma, J. Ropponen (2018) Injection Molding of Thermoplastic Cellulose Esters and Their Compatibility with Poly(Lactic Acid) and Polyethylene. Materials 11:13. https://doi.org/10.3390/ma11122358
8. M.D. Zuo, N.Y. Pan, Q.J. Liu, X.H. Ren, Y. Liu, T.S. Huang (2020) Three-dimensionally printed polylactic acid/cellulose acetate scaffolds with antimicrobial effect. Rsc Adv 10:2952-2958. https://doi.org/10.1039/c9ra08916k
9. S.F. Gomaa, T.M. Madkour, S. Moghannem, I.M. El-Sherbiny (2017) New polylactic acid/ cellulose acetate-based antimicrobial interactive single dose nanofibrous wound dressing mats. Int J Biol

Macromol 105:1148-1160. https://doi.org/10.1016/j.ijbiomac.2017.07.145

10. M. Khodayari, A.A. Basti, A. Khanjari, A. Misaghi, A. Kamkar, P.M. Shotorbani, H. Hamedi (2019) Effect of poly(lactic acid) films incorporated with different concentrations of Tanacetum balsamita essential oil, propolis ethanolic extract and cellulose nanocrystals on shelf life extension of vacuum-packed cooked sausages. Food Packag Shelf Life 19:200-209. https://doi.org/10.1016/j.fpsl.2018.11.009
11. H.-M. Wang, Y.-T. Chou, C.-S. Wu, J.-T. Yeh (2012) Polyester/cellulose acetate composites: Preparation, characterization and biocompatible. J Appl Polym Sci 126:242-251. https://doi.org/10.1002/app.36965
12. M. Boulven, G. Quintard, A. Cottaz, C. Joly, A. Charlot, E. Fleury (2019) Homogeneous acylation of Cellulose diacetate: Towards bioplastics with tuneable thermal and water transport properties. Carbohydr Polym 206:674-684. https://doi.org/10.1016/j.carbpol.2018.11.030
13. S. Abu Aldam, M. Dey, S. Javaid, Y. Ji, S. Gupta (2020) On the Synthesis and Characterization of Polylactic Acid, Polyhydroxyalkanoate, Cellulose Acetate, and Their Engineered Blends by Solvent Casting. J Mater Eng Perform 29:5542-5556. https://doi.org/10.1007/s11665-020-04594-3
14. A.S. Volokhova, J.B. Waugh, K.J. Arrington, J.B. Matson (2019) Effects of graft polymer compatibilizers in blends of cellulose triacetate and poly(lactic acid). Polym Int 68:1263-1270. https://doi.org/10.1002/pi.5820
15. M.B. Coltelli, N. Mallegni, S. Rizzo, S. Fiori, F. Signori, A. Lazzeri (2021) Compatibilization of Poly(Lactic Acid) (PLA)/Plasticized Cellulose Acetate Extruded Blends through the Addition of Reactively Extruded Comb Copolymers. Molecules 26:20. https://doi.org/10.3390/molecules26072006
16. M.B. Coltelli, N. Mallegni, S. Rizzo, P. Cinelli, A. Lazzeri (2019) Improved Impact Properties in Poly(lactic acid) (PLA) Blends Containing Cellulose Acetate (CA) Prepared by Reactive Extrusion. Materials 12:20. https://doi.org/10.3390/ma12020270
17. B.-U. Nam, K.-D. Min, Y. Son (2015) Investigation of the nanostructure, thermal stability, and mechanical properties of polylactic acid/cellulose acetate butyrate/clay nanocomposites. Mater Lett 150:118-121. https://doi.org/10.1016/j.matlet.2015.03.019
18. C. Devi, S. Narayanan (2019) Poly (amido amine) dendrimer/silver nanoparticles/multi-walled carbon nanotubes/poly (neutral red)-modified electrode for electrochemical determination of paracetamol. Ionics 25. https://doi.org/10.1007/s11581-018-2609-0
19. A. Pistone, D. Iannazzo, C. Celesti, C. Scolaro, S.V. Giofré, R. Romeo, A. Visco (2020) Chitosan/PAMAM/Hydroxyapatite Engineered Drug Release Hydrogels with Tunable Rheological Properties. Polymers 12. https://doi.org/10.3390/polym12040754
20. F. Abedi-Gaballu, G. Dehghan, M. Ghaffari, R. Yekta, S. Abbaspour-Ravasjani, B. Baradaran, J. Ezzati Nazhad Dolatabadi, M.R. Hamblin (2018) PAMAM dendrimers as efficient drug and gene delivery nanosystems for cancer therapy. Appl Mater Today 12:177-190. https://doi.org/10.1016/j.apmt.2018.05.002

21. A.H. Shah, I. Djordjevic, T.W.J. Steele (2020) Tertiary blends of PAMAM/PEG/PEG tissue bioadhesives. J Mech Behav Biomed Mater 101:103405 https://doi.org/10.1016/j.jmbbm.2019.103405.
22. W. Qin, G. Qian, H. Tao, J. Wang, J. Sun, X. Cui, Y. Zhang, X. Zhang (2019) Adsorption of Hg(II) ions by PAMAM dendrimers modified attapulgite composites. React Funct Polym 136:75-85. https://doi.org/10.1016/j.reactfunctpolym.2019.01.005
23. C.J. Wei, L.G. Lin, Y.P. Zhao, X.Y. Zhang, N. Yang, L. Chen, X.J. Huang (2020) Fabrication of pH-Sensitive Superhydrophilic/Underwater Superoleophobic Poly(vinylidene fluoride)-graft-(SiO2 Nanoparticles and PAMAM Dendrimers) Membranes for Oil-Water Separation. ACS Appl Mater Interfaces 12:19130-19139. https://doi.org/ 10.1021/acsami.9b22881.
24. Y. Du, X. Wang, D. Lian, Y. Liu, L. Zhang, S. Xu, S. Cao (2020) Dendritic PAMAM polymers for strong perovskite intergranular interaction enhancing power conversion efficiency and stability of perovskite solar cells. Electrochimica Acta 349:136387. https://doi.org/10.1016/j.electacta.2020.136387
25. H. He, T. Zhang, Y. Yang (2021) A facile way to modify carbon fibers and its effect on mechanical properties of epoxy composites. J Mater Res Technol 10:164-174. https://doi.org/10.1016/j.jmrt.2020.12.007
26. Y.J. Jin, Y.X. Weng, X.X. Li, M. Zhang, X.L. Xin (2015) Effect of blending with polyamidoamine (PAMAM) dendrimer on the toughness of poly(hydroxybutyrate-co-hydroxyvalerate) (PHBV). J Mater Sci 50:794-800. https://doi.org/ 10.1007/s10853-014-8639-8.
27. X. Liu, Y. Sheng, D. Wu, R. Zhang, H. Cui (2019) Synthesis of PAMAM-GO as new nanofiller to enhance the crystallization properties of polylactic acid. Mater Lett 235:27-30. https://doi.org/10.1016/j.matlet.2018.09.154
28. W. Wang, T. Liang, H. Bai, W. Dong, X. Liu (2018) All cellulose composites based on cellulose diacetate and nanofibrillated cellulose prepared by alkali treatment. Carbohydr Polym 179:297-304. https://doi.org/10.1016/j.carbpol.2017.09.098
29. A. Ibrahim, A. Zikry, T. Madkour (2017) Enhanced thermal stability of "environmentally friendly" biodegradable poly(lactic acid) blends with cellulose acetate. An experimental and molecular modeling study. Biointerface Res Appl Chem 7:2230-2237.
30. M.A. Laadila, K. Hegde, T. Rouissi, S.K. Brar, R. Galvez, L. Sorelli, R.B. Cheikh, M. Paiva, K. Abokitse (2017) Green synthesis of novel biocomposites from treated cellulosic fibers and recycled bio-plastic polylactic acid. J Clean Prod 164:575-586. https://doi.org/10.1016/j.jclepro.2017.06.235
31. S.S. Shazleen, T.A.T. Yasim-Anuar, N.A. Ibrahim, M.A. Hassan, H. Ariffin (2021) Functionality of Cellulose Nanofiber as Bio-Based Nucleating Agent and Nano-Reinforcement Material to Enhance Crystallization and Mechanical Properties of Polylactic Acid Nanocomposite. Polymer 13:19. https://doi.org/10.3390/polym13030389
32. J. Kuang, J.H. Wang, Y. Bai, Y. Li (2019) Effects and mechanism of cellulose acetate butyrate on the crystallization of polylactic acid. Eur Polym J 121:109286. https://doi.org/10.1016/j.eurpolymj.2019.109286.

33. D. Kang, H.-I. Kim (2021) Improvement in nano-pattern replication of injection molding by polyamide/dendrimer blend. Polym Eng Sci 61:822-829. https://doi.org/10.1002/pen.25627
34. N. Herrera, A.P. Mathew, K. Oksman (2015) Plasticized polylactic acid/cellulose nanocomposites prepared using melt-extrusion and liquid feeding: Mechanical, thermal and optical properties. Compos Sci Technol 106:149-155. https://doi.org/10.1016/j.compscitech.2014.11.012
35. E. Fortunati, D. Puglia, J.M. Kenny, M. Minhaz-Ul Haque, M. Pracella (2013) Effect of ethylene-co-vinyl acetate-glycidylmethacrylate and cellulose microfibers on the thermal, rheological and biodegradation properties of poly(lactic acid) based systems. Polym Degrad Stab 98:2742-2751. https://doi.org/10.1016/j.polymdegradstab.2013.10.007
36. Y. Boonluksiri, B. Prapagdee, N. Sombatsompop (2021) Promotion of polylactic acid biodegradation by a combined addition of PLA-degrading bacterium and nitrogen source under submerged and soil burial conditions. Polym Degrad Stab 188:109562. https://doi.org/10.1016/j.polymdegradstab.2021.109562
37. Y. Ahmadzadeh, A. Babaei, A. Goudarzi (2018) Assessment of localization and degradation of ZnO nano-particles in the PLA/PCL biocompatible blend through a comprehensive rheological characterization. Polym Degrad Stab 158:136-147. https://doi.org/10.1016/j.polymdegradstab.2018.10.007
38. A. Ganjalinia, S. Akbari, A. Solouk (2021) Tuning poly (L-lactic acid) scaffolds with poly(amidoamine) and poly(propylene imine) dendrimers: surface chemistry, biodegradation and biocompatibility. J Macromol Sci A Pure Appl Chem. https://doi.org/10.1080/10601325.2021.1880935
39. B. Srinageshwar, M. Florendo, B. Clark, K. Johnson, N. Munro, S. Peruzzaro, A. Antcliff, M. Andrews, A. Figacz, D. Swanson, G.L. Dunbar, A. Sharma, J. Rossignol (2020) A Mixed-Surface Polyamidoamine Dendrimer for In Vitro and In Vivo Delivery of Large Plasmids. Pharm 12. https://doi.org/10.3390/pharmaceutics12070619

Figures

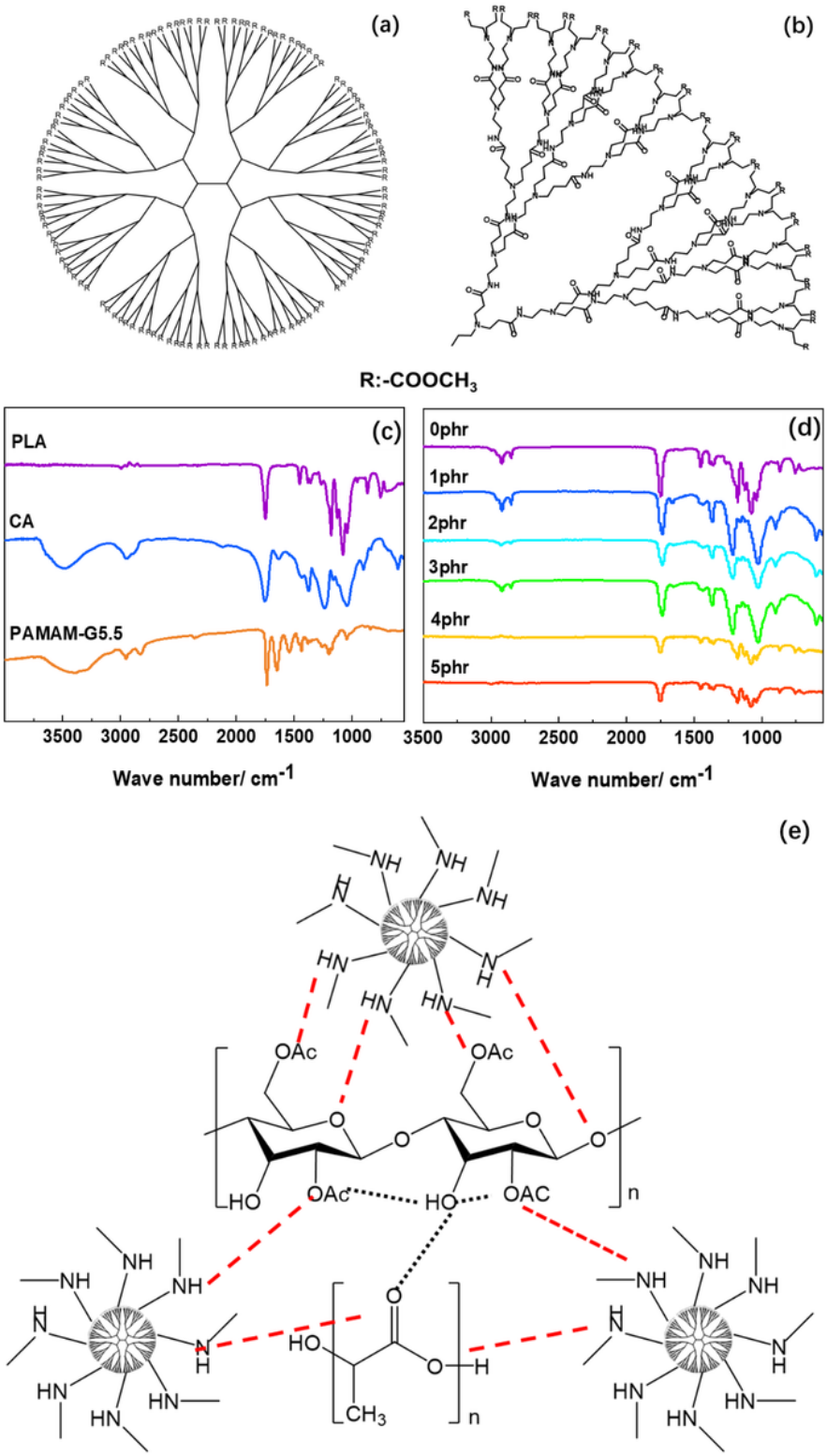

Figure 1

The structure diagram of PAMAM (a, b), FT-IR spectra of PLA / CA blends with different content of PAMAM (c, d) and the interaction mechanism of PAMAM with PLA and CA (e).

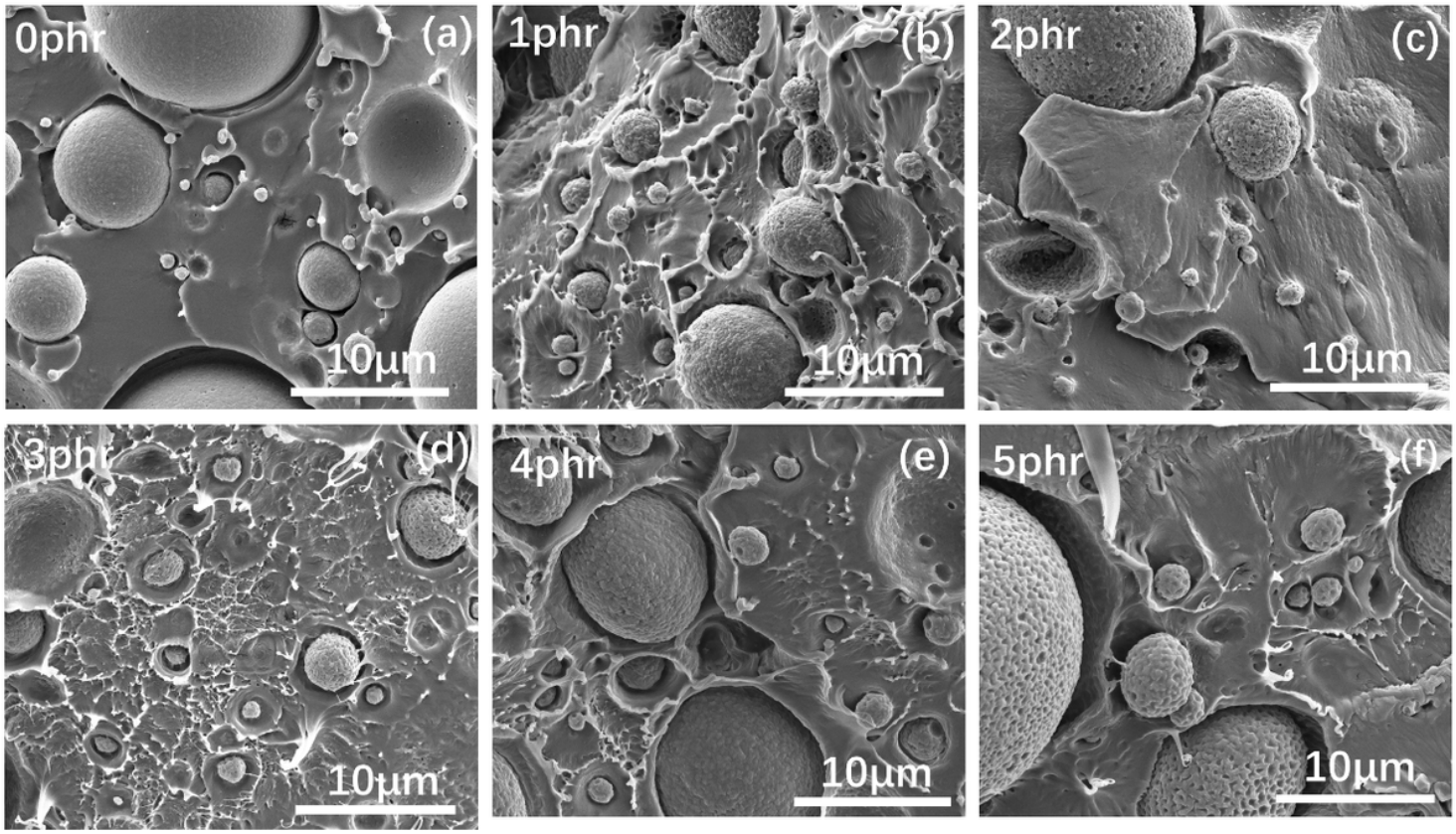

Figure 2

SEM images of the PLA / CA blends with different content of PAMAM: (a) 0phr, (b) 1 phr, (c) 2 phr, (d) 3 phr, (e) 4 phr, (f) 5 phr.

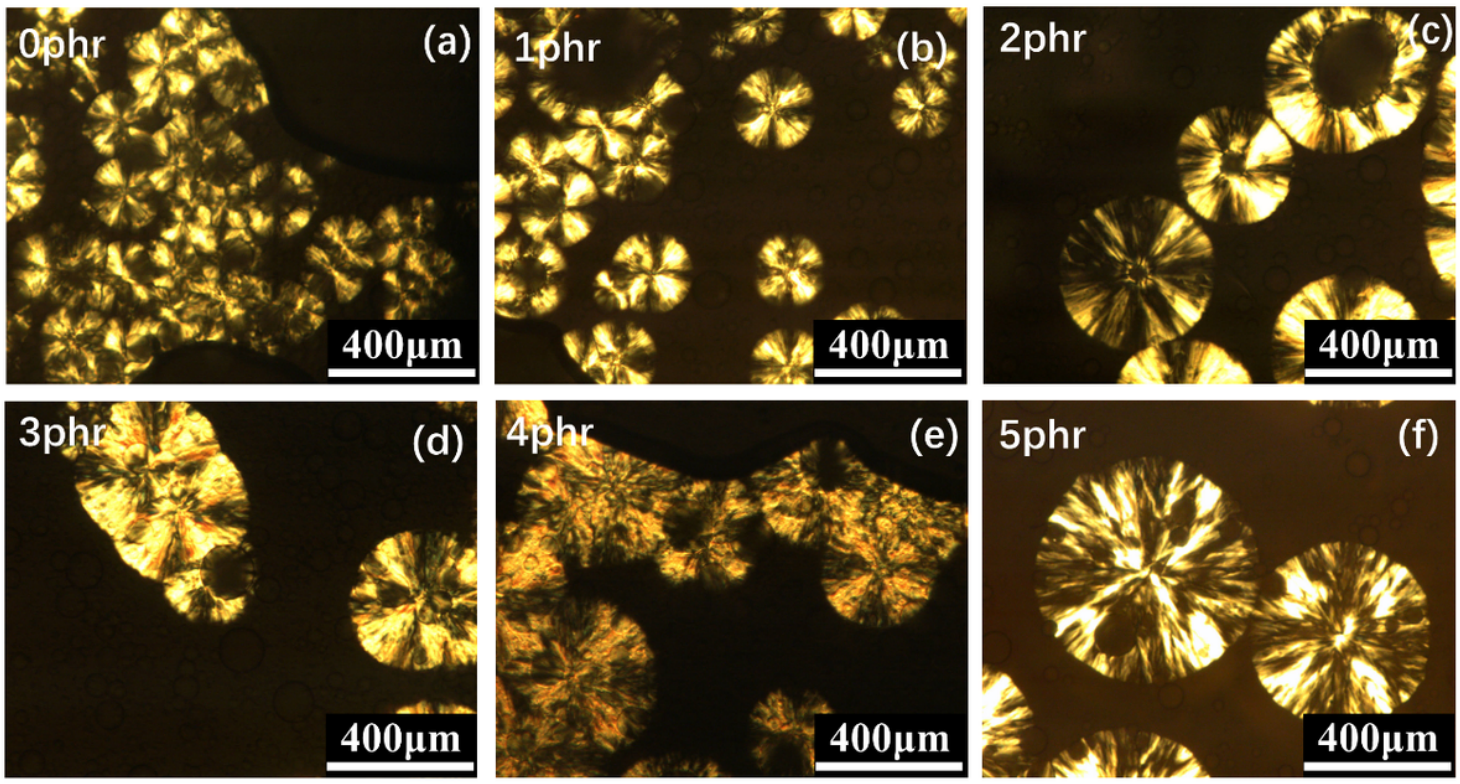

Figure 3

Polarization diagram of PLA / CA blends system with PAMAM for isothermal crystallization: (a) 0 phr; (b) 1 phr; (c) 2 phr; (d) 3 phr; (e) 4 phr; (f) 5 phr.

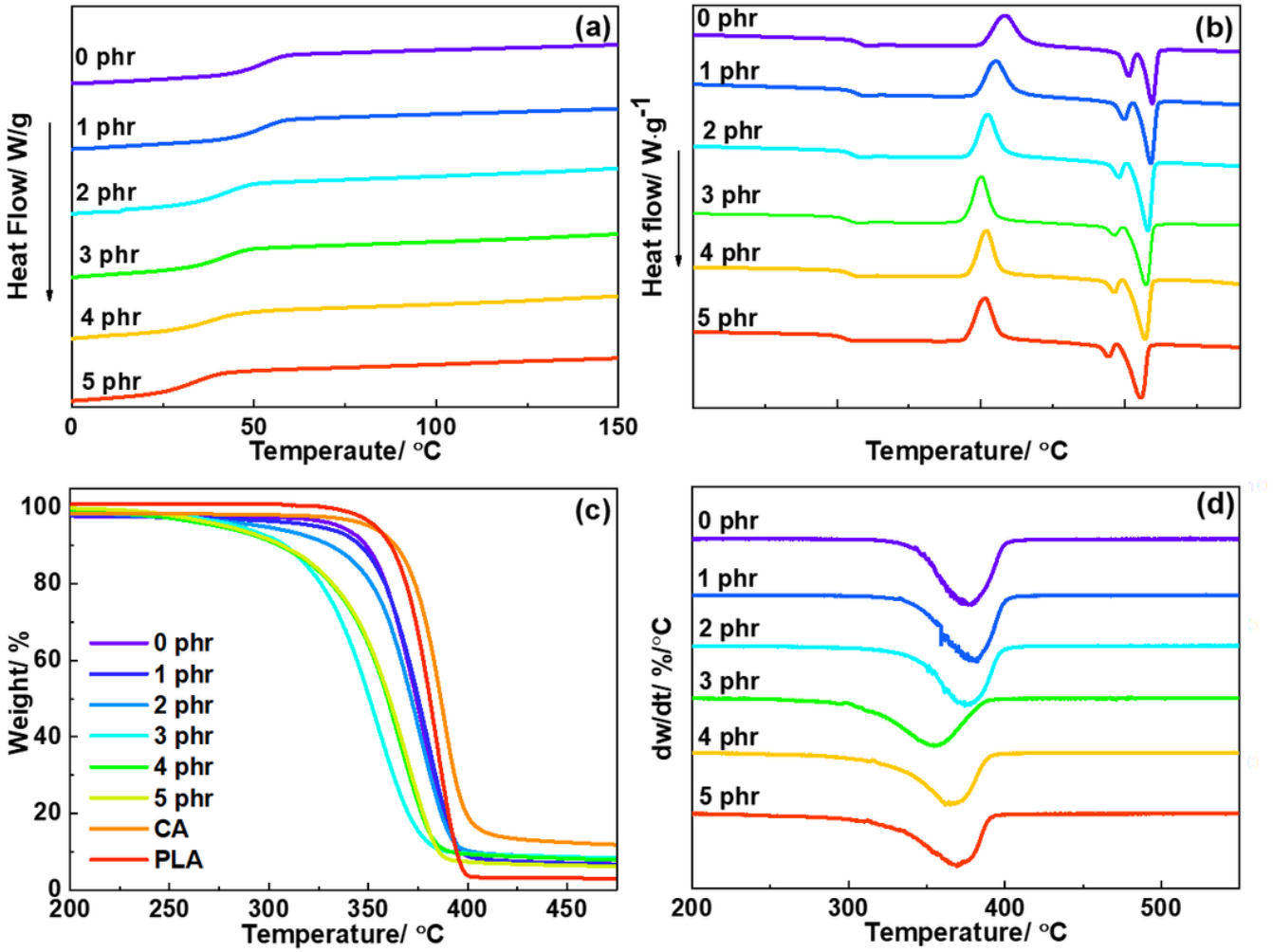

Figure 4

The (a) cooling, (b) second heating DSC curves, (c) TG, (d) DTG curves of the PLA/CA blends with different content of PAMAM.

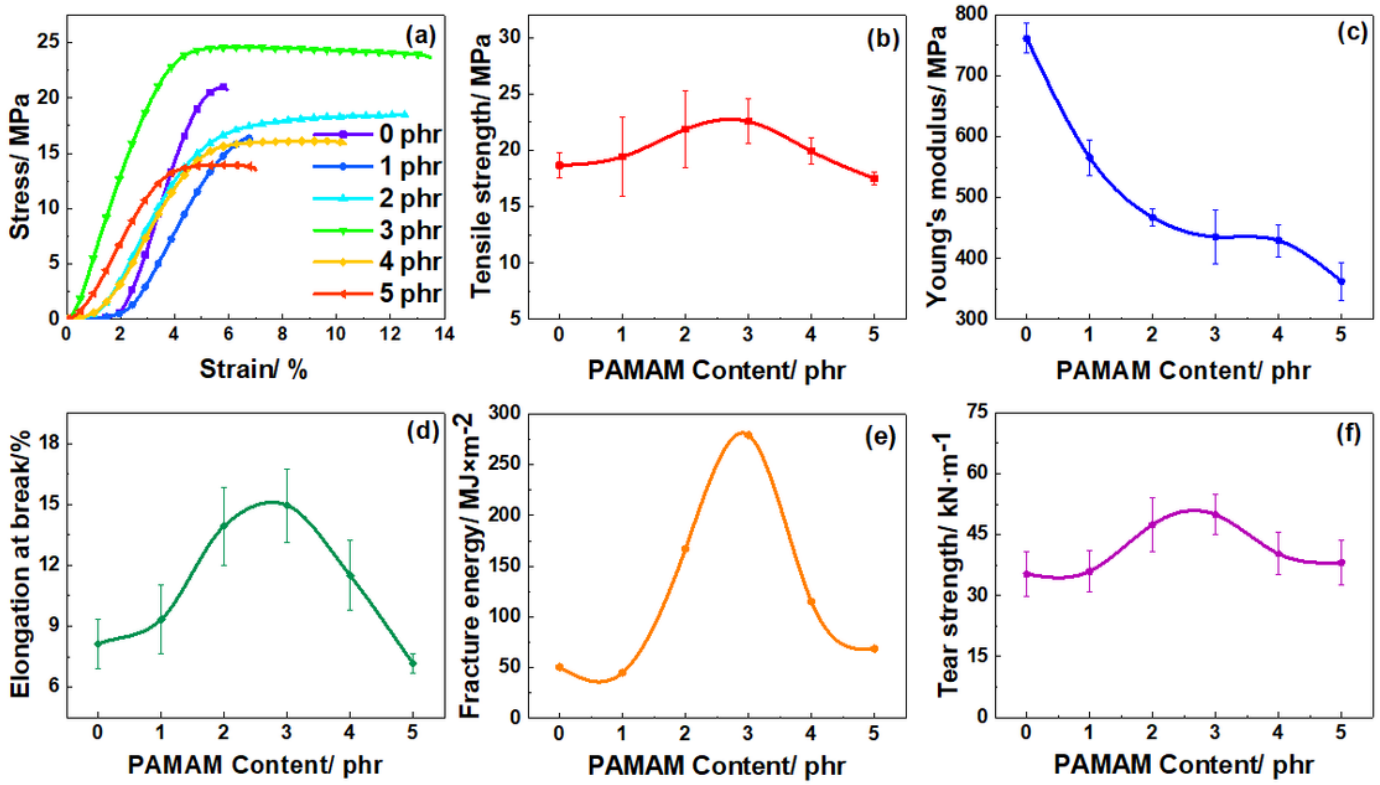

Figure 5

Mechanical properties of the PLA/CA blends with different content of PAMAM:(a) typical stress-strain curves, (b) tensile strength, (c) Young's modulus, (d) elongation at break, (e) fracture energy, (f) tear strength.

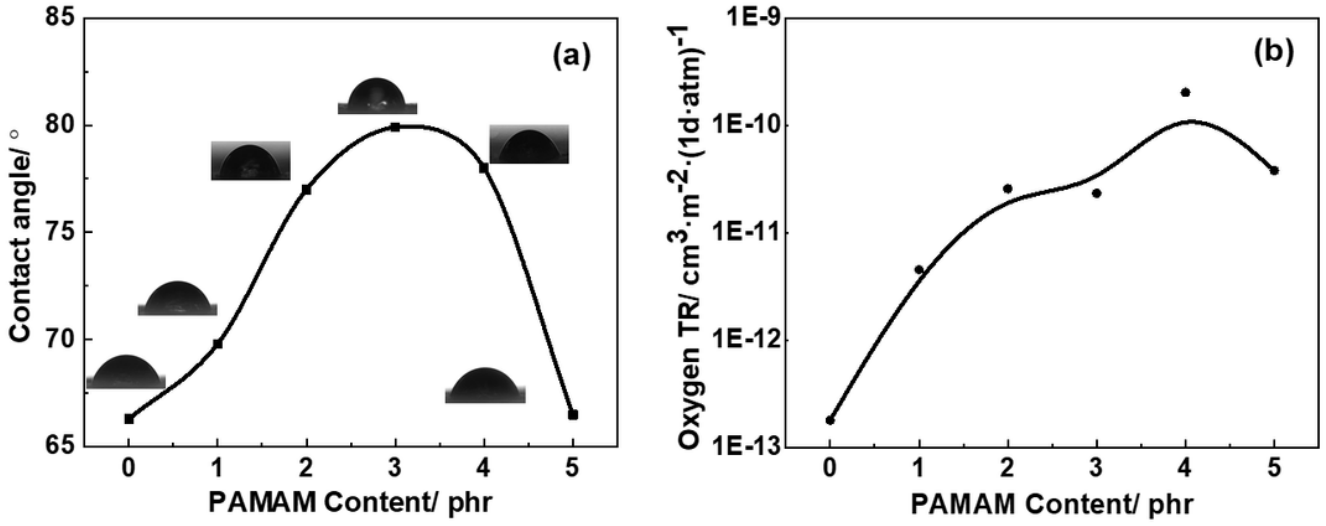

Figure 6

Hydrophilicity and gas permeability of the PLA/CA blends with different content of PAMAM: (a) contact angle; (b) oxygen permeability coefficient.

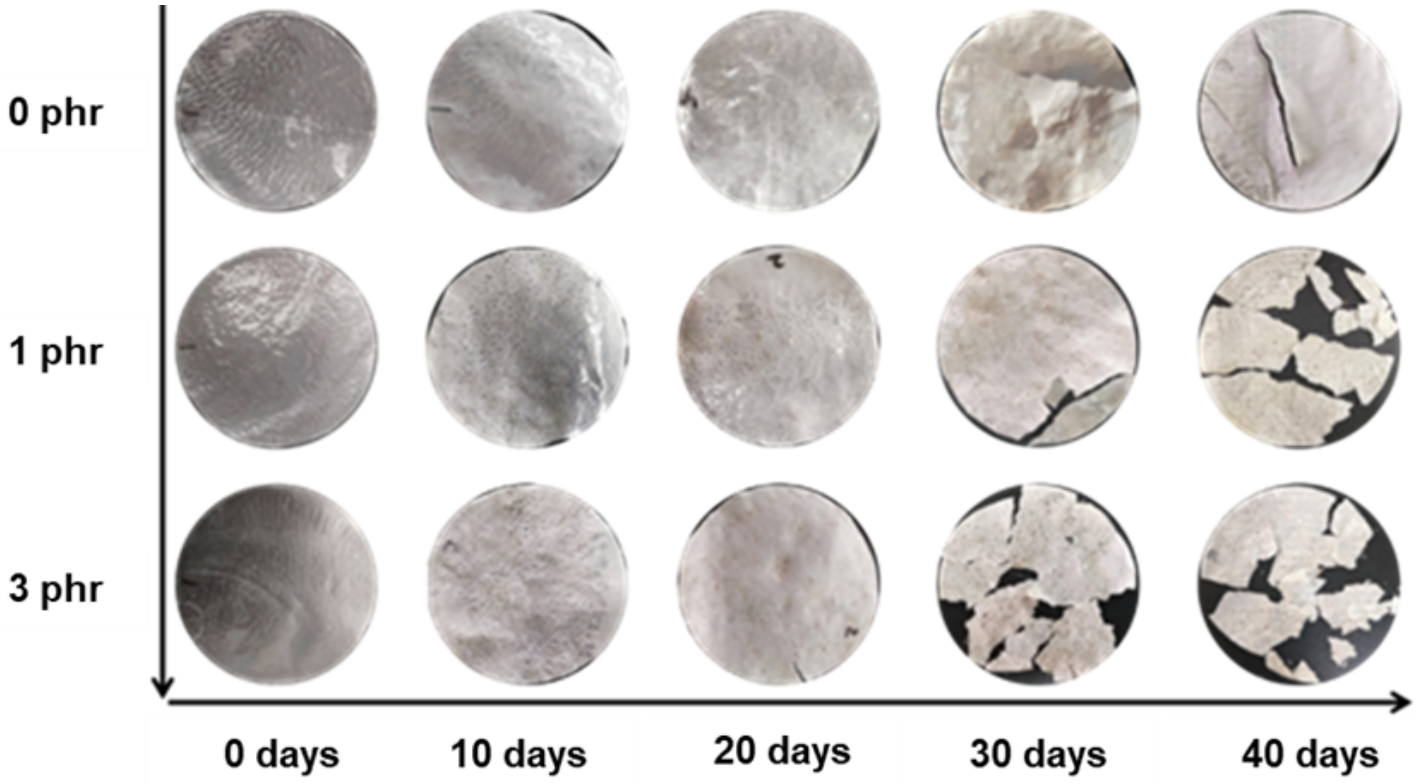

Figure 7

Photos of PLA / CA blends during degradation.

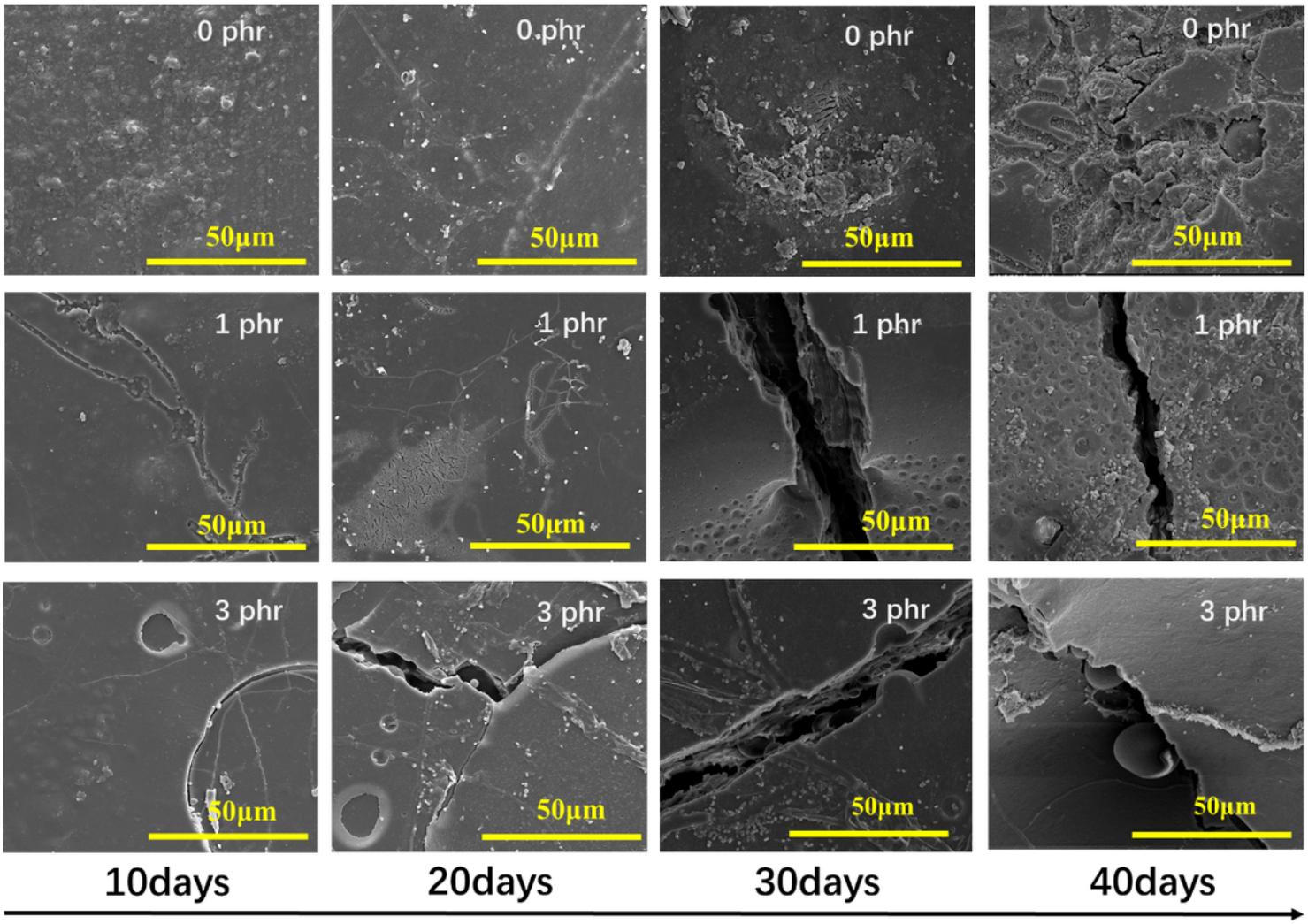

Figure 8

SEM images of the degradation process of PLA / CA blends.

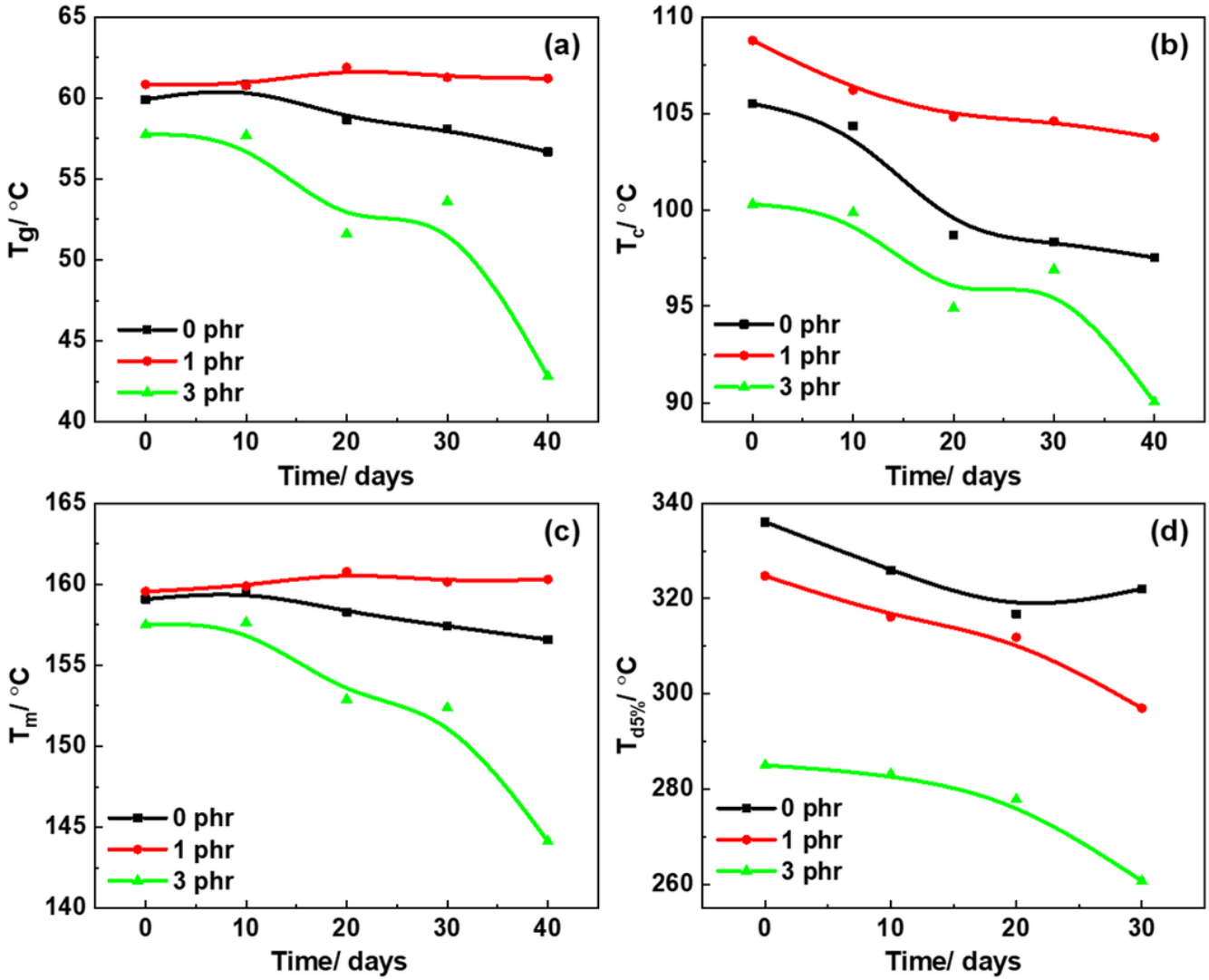

Figure 9

Tg (a), Tc (b), Tm (c) and Td5% (d) of PLA / CA blends during degradation.

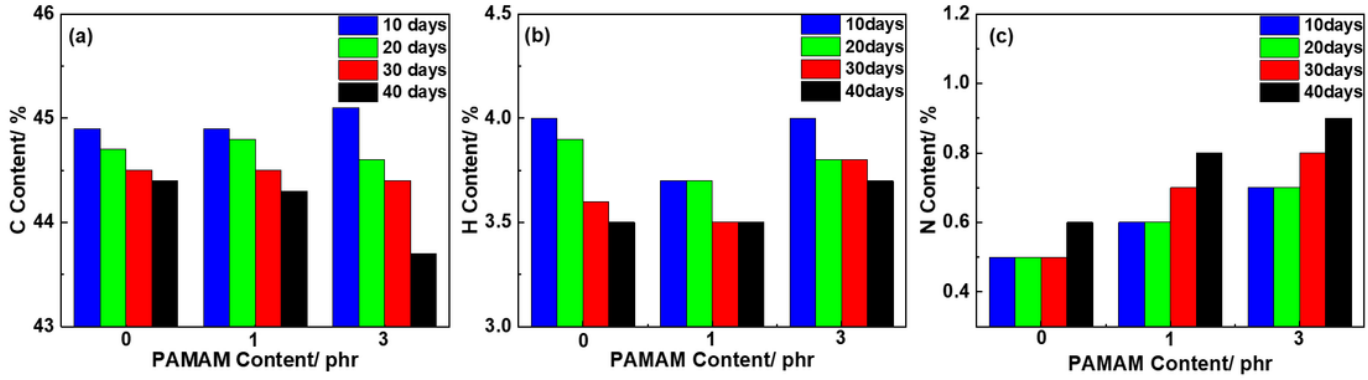

Figure 10

Different elements ((a) C, (b) H, (c) N) contents of PLA / CA blends with PAMAM addition during degradation.

Supplementary Files

This is a list of supplementary files associated with this preprint. Click to download.

- SupplementaryMaterialf.docx